

Sub-Nyquist Radar Prototype: Hardware and Algorithm

ELIAHU BARANSKY

GAL ITZHAK

NOAM WAGNER

IDAN SHMUEL

ELI SHOSHAN

YONINA ELDAR, Fellow, IEEE

Technion

Israel

Traditional radar sensing typically employs matched filtering between the received signal and the shape of the transmitted pulse. Matched filtering (MF) is conventionally carried out digitally, after sampling the received analog signals. Here, principles from classic sampling theory are generally employed, requiring that the received signals be sampled at twice their baseband bandwidth. The resulting sampling rates necessary for correlation-based radar systems become quite high, as growing demands for target distinction capability and spatial resolution stretch the bandwidth of the transmitted pulse. The large amounts of sampled data also necessitate vast memory capacity. In addition, real-time data processing typically results in high power consumption. Recently, new approaches for radar sensing and estimation were introduced, based on the finite rate of innovation (FRI) and Xampling frameworks. Exploiting the parametric nature of radar signals, these techniques allow significant reduction in sampling rate, implying potential power savings, while maintaining the system's estimation capabilities at sufficiently high signal-to-noise ratios (SNRs). Here we present for the first time a design and implementation of an Xampling-based hardware prototype that allows sampling of radar signals at rates much lower than Nyquist. We demonstrate by real-time analog experiments that our system is able to maintain reasonable recovery capabilities, while sampling radar signals that require sampling at a rate of about 30 MHz at a total rate of 1 MHz.

I. INTRODUCTION

The classic radar sensing problem treats detection of targets moving in space. This is achieved by transmitting RF pulses of electromagnetic energy and sampling the signals caused by their reflection. The samples are then processed, in an attempt to determine the targets' location in space and their velocity. Traditional processing methods in both literature and practice involve a preliminary stage, referred to as matched filtering (MF) or pulse compression [1, 2], in which the transmitted pulse is correlated with the received signal. For the problem of detecting targets in white Gaussian noise, the MF is known to maximize the effective signal-to-noise ratio (SNR).

The MF stage is typically carried out digitally, after sampling the detected analog signal. Classic Shannon-Nyquist sampling theory [3] guarantees full recovery of a general bandlimited analog signal from samples taken at twice its baseband bandwidth. However, applying this framework to modern radar systems typically results in extremely high sampling rates, due to the wide bandwidth characteristic of the sampled signals. The latter is a direct consequence of the well-known relationship between a radar system's resolution and the bandwidth of the transmitted signals.

Formulating the radar problem as one of parametric inference, one may show that Nyquist sampling is, in fact, a redundant approach for resolving the desired parameters. Nonetheless, this method is still widely employed by modern radar systems, to a large extent because it produces a straightforward and simple solution to the parametric inference problem as well as to the preceding analog sampling stage. However, the growing sampling rates required due to the desire to increase resolution necessitate sophisticated analog front ends and imply higher power consumption and vast memory capacity.

Recently, new approaches [4] to radar processing were introduced, which allow practical solution of the parametric problem, from a small number of measurements taken after appropriate analog prefiltering. The estimation problem is solved in the frequency domain using known tools from array processing [5], with the necessary number of measurements typically much smaller than that obtained by Nyquist sampling. Related works [6–8] treat ultrasound signal sampling and are readily adapted to the radar scenario. These methods are based on the finite rate of innovation (FRI) [9] and Xampling [10, 11] approaches. The FRI framework treats sampling and recovery of signals characterized by a finite number of degrees of freedom per unit time and is based on connecting sampling theory with array processing methods. In many cases such signals can be sampled and recovered at a rate proportional to the number of unknowns per time interval, which is usually much lower than the Nyquist rate. The Xampling philosophy ties together sub-Nyquist sampling based on analog preprocessing with techniques of compressed sensing (CS) [12–14] for recovery. However, as discussed in the

Manuscript received August 4, 2012; revised June 14, 2013, November 3, 2013; released for publication December 26, 2013.

DOI. No. 10.1109/TAES.2014.120475.

Refereeing of this contribution was handled by T. Strohmer.

Authors' addresses: E. Baransky, HaShiryon St. 5, Kiryat Gat, Israel, 82202. E-mail: (elibj123@gmail.com), G. Itzhak, HaSanhadryn, St. 22, Holon, Israel 58 581; N. Wagner, Yehiam St. 6/2, Karmiel, Israel, 2182303; I. Shmuel, E. Shoshan, Y. Eldar, Dept. of Electrical Engineering, Technion City, Haifa, Israel 32 000.

following sections, these approaches typically require sophisticated sampling schemes, which acquire generalized measurements of the analog signals.

Here we present a concrete analog-to-digital conversion (ADC) scheme and a recovery algorithm with relaxed constraints for sampling radar signals at sub-Nyquist rates. Our processing is based on a frequency-domain formulation of the problem. As we show, a small number of frequency samples of the received signal carry sufficient information about the parameters of interest. Our prototype allows to obtain these needed frequency coefficients directly from the analog input using simple analog filters and low rate sampling. The results of [15] establish that a single delay can be found efficiently from random frequency samples in the presence of noise providing theoretical justification to our approach. The use of frequency samples for CS of signals sparse in time is also studied in [16].

In order to choose appropriate frequencies to process we connect our problem to that of beampattern design in array processing, and rely on ideas obtained in that context. In particular, it is known in the array processing literature that random frequencies spread over a wide aperture lead to good performance [17, 18]. However, in the context of ADC design this choice corresponds to a complicated receiver structure. Instead, we show that choosing several random groups of coefficients can yield similar performance, while resulting in a simple ADC structure.

Our hardware prototype implements a combination of the multichannel topology suggested in [7] and the filtering approach presented in [6], additionally taking into account the practical challenges they impose. In particular, our board consists of 4 channels, each comprising a bandpass crystal filter with a random effective carrier frequency. This allows to obtain a wide spread of Fourier coefficients of the signal in an efficient manner. The proposed recovery algorithm obtains the delays and amplitudes of the radar signal from these coefficients.

Using crystal filters, which have extremely narrow transition bands, we are able to obtain a sufficient amount of information from the signal, while substantially decreasing the total sampling rate, as discussed in Section III. Since crystal filters are standard, off-the-shelf components, we are confined to adapt our channel design to their properties, in order to maximize their efficiency. We discuss the challenges this imposes and our method for overcoming them in Section III.

Simulations as well as real-time experiments of our hardware prototype prove high target hit-rate and location estimation capabilities for preintegration SNR values over -14 dB, with a large reduction factor in sampling rate compared with Nyquist sampling. In fact, standard radar systems, in which Nyquist sampling is employed for solving the parametric inference problem, typically oversample the received signals, due to the nonideal behavior of practical antialiasing filters. With respect to the resulting sampling rates, we achieve a thirty-fold

reduction using our approach. That is, our system operates at a total sampling rate of 1 MHz (20 times less than the signal's Nyquist rate), while an MF-based system would typically operate at a rate of 30 MHz (requiring an oversampling factor of 1.5 in order to use practical filters). We are able to achieve this reduction without substantially degrading the target hit-rate and location estimation capabilities, provided that the system operates at sufficiently high SNR. For instance, we achieved target hit-rate of approximately 90% for preintegration SNRs larger than -12 dB.

To estimate the underlying sparse structure, or the targets in our setting, from the selected Fourier coefficients of the received signal, previous work in the FRI framework traditionally employed spectral estimation techniques. Here, we use a CS formulation of the recovery stage, as suggested in [18]. In CS, the signal is assumed to have a sparse representation in a discrete basis. An extensive search for the best sparse representation results in combinatorial run-time complexity, which is impractical for real-time applications such as radar sensing. Many polynomial-time algorithms have been proposed that can be shown to recover the true sparse vector under appropriate conditions [13]. In our simulations, we use the orthogonal matching pursuit (OMP) algorithm [19, 20].

There have been several other works that employ CS algorithms in the context of radar signal processing such as [21–26]. However, these papers either do not address sample rate reduction and continue sampling at the Nyquist rate, or they assume that a smaller number of samples has been obtained but do not address how to subsample the analog received signal using practical ADCs. Furthermore, previous CS-based methods typically impose constraints on the radar transmitter, which are not needed in our approach. An alternative architecture proposed in the CS literature to sample signals at sub-Nyquist rates is the random demodulator [27–29]. This receiver consists of parallel channels that multiply the incoming signal with a set of random binary sequences. A similar concept is used in the modulated wideband converter of [10]. These techniques are particularly suited to signals that are sparse in frequency, while here we focus on signals with a small number of parameters in the time domain.

The remainder of the paper is organized as follows. Section II establishes the mathematical foundation of our techniques. We present the radar signal model, link several CS concepts to our application, and provide justification for the chosen parameters. Section III compares different analog sampling implementations. These systems offer a compromise between theoretical requirements and practical hardware constraints. We then elaborate on our choice of hardware design. Finally, in Section IV we present results of MATLAB hardware simulations, as well as results of real-time hardware experiments. We also describe our realization environment, and conclude by discussing the overall system performance.

II. SAMPLING OF RADAR SIGNALS

A. Methodology

Radar systems estimate target locations by transmitting periodic pulses and processing their reflections. We model the received radar signal as the following stream of pulses:

$$x(t) = \sum_{n=0}^{M-1} \sum_{l=1}^L a_l h(t - nT - t_l), \quad a_l \in \mathbb{C}, \quad t_l \in [0, T], \quad (1)$$

where T is the radar's pulse repetition interval (PRI) and M is the number of transmitted pulses. This model complies with monostatic radars, with nonfluctuating point targets assumed to be stationary or moving at very slow velocities, so that no Doppler shift is incorporated into the model. We show how to adapt the results to allow for Doppler processing in [30]. The parameters $\{a_l, t_l\}_{l=1}^L$ correspond to the estimated pulses' amplitudes and delays, respectively, and are proportional to the targets' distance from the receiver and their radar cross section (RCS). We assume that the shape of the pulse $h(t)$ and the maximal number of echoes L are known, although future research may relax this constraint. In particular, knowledge of L is used to simplify the stopping criteria of our reconstruction algorithm, but is not essential.

Traditional radar systems sample the received signal at the Nyquist rate, determined by the baseband bandwidth of $h(t)$. Our goal is to recover $x(t)$ from its samples taken far below this rate. It is readily seen that $x(t)$ is completely defined by at most $2L$ unknown parameters, namely a_l and t_l , within any length- T time interval. Hence, in the absence of noise, one would expect to be able to accurately recover $x(t)$ from only $2L$ samples per time T [9]. If L/T is sufficiently small with respect to $h(t)$'s bandwidth, then this implies a significant reduction in sampling rate. Since radar signals tend to be sparse in the time domain, simply acquiring $2L$ data samples at a low rate will not generally yield adequate recovery. Indeed, if the separation between samples is larger than the effective spread in time, then with high probability many of the samples will be close to zero and will not contain any information. This implies that presampling analog processing must be performed in order to smear the signal in time before low rate sampling.

As shown in [9, 6, 7], the $2L$ unknowns defining $x(t)$ may be recovered from only $2L$ measurements, corresponding to the projection of $x(t)$ onto a subset of its Fourier series coefficients. Calculated with respect to a single period $[0, T)$, these coefficients are given by

$$\begin{aligned} X[k] &= \frac{1}{T} \int_{-\infty}^{\infty} \left[\sum_{l=1}^L a_l h(t - t_l) \right] e^{-j \frac{2\pi}{T} kt} dt \\ &= \frac{1}{T} \sum_{l=1}^L a_l \int_{-\infty}^{\infty} h(t - t_l) e^{-j \frac{2\pi}{T} kt} dt \\ &= \frac{1}{T} H\left(\frac{2\pi}{T} k\right) \sum_{l=1}^L a_l e^{-j \frac{2\pi}{T} kt_l}, \end{aligned} \quad (2)$$

where $H(\omega)$ is the continuous-time Fourier transform (CTFT) of the pulse. Choosing the coefficients such that $H\left(\frac{2\pi}{T} k\right)$ is non-zero, (2) can be rewritten as

$$Y[k] = \frac{X[k]}{\frac{1}{T} H\left(\frac{2\pi}{T} k\right)} = \sum_{l=1}^L a_l e^{-j \frac{2\pi}{T} kt_l}, \quad (3)$$

which is a standard sum-of-exponentials problem studied extensively in the array processing literature. It can be shown that this problem has a unique solution given $K \geq 2L$ coefficients $Y[k]$ [9]. We discuss hardware prototypes to acquire these measurements efficiently in Section III. The remainder of this section is devoted to reviewing algorithmic approaches for solving (3).

B. Recovery Algorithm

Many mature techniques for solving (3) exist, including matrix pencil (MP) [31], annihilating filter [9], and others that can be found in [5]. These algorithms arise from spectral analysis methods, and generally require the measurements to form a consecutive subset of the signal's Fourier coefficients. An exception is the MUSIC algorithm, which can be applied on any set of coefficients [32]. While these techniques work well at high SNR; their performance deteriorates at low SNR values.

In [8] it was suggested to use a nonconsecutive set of Fourier coefficients selected in a distributed manner, as many detection systems (such as ultrasound in [8] and radar in our work) benefit from wide frequency aperture. While consecutive coefficients can be obtained using a simple low-pass filter (LPF), it is shown in [8] that a distributed selection results in better recovery and noise robustness. In order to remove the constraint of consecutive selection, and improve performance in low SNR, we choose to employ a CS formulation of (3) for recovery.

We begin by quantizing the analog time axis with a resolution step of Δ , thus, approximating (3) as

$$Y[k] \approx \sum_{l=1}^L a_l e^{-j \frac{2\pi}{T} kn_l \Delta}, \quad 0 \leq n_l < N, \quad (4)$$

where $N = T/\Delta$ is the number of bins in the PRI and $t_l \approx n_l \Delta$ is the discrete approximation of the time delays. Selecting a finite subset of K measurements, $\kappa = \{k_1, k_2, \dots, k_K\} \subset \{0, \dots, N-1\}$, (4) may be written as

$$\mathbf{y} = \mathbf{Ax}. \quad (5)$$

Here $\mathbf{y} \in \mathbb{C}^K$ is the vector of measurements $Y[k]$, \mathbf{A} is a $K \times N$ matrix with ℓ th element $\exp\{-j2\pi k_\ell n_l / N\}$, formed by taking the set κ of rows from an $N \times N$ discrete Fourier transform (DFT) matrix, and $\mathbf{x} \in \mathbb{C}^N$ is an L -sparse vector with non-zero entries at indices $\{n_l\}_{l=1}^L$. In the context of CS, \mathbf{A} is known as the sensing matrix.

Our goal is to find the non-zero entries of \mathbf{x} from the measurements \mathbf{y} . This is a standard CS problem, with \mathbf{A} being a partial Fourier matrix. A solution can be obtained,

for example, by using the well-known OMP algorithm. This method iteratively finds the non-zero entries of \mathbf{x} by seeking the maximal absolute correlations between \mathbf{y} and the columns of \mathbf{A} , while maintaining an orthogonalization step at the end of each iteration [20, 19]. To further improve performance, we used a variation of the standard OMP, where we computed the maximal correlation using the pseudoinverse $\mathbf{A}^\dagger = (\mathbf{A}^H \mathbf{A})^{-1} \mathbf{A}^H$ rather than the inner product.

Once the non-zero entries are found, the time delays are directly calculated while the amplitudes are estimated via standard least-squares. A pseudocode of the recovery algorithm is given in Algorithm 1.

ALGORITHM 1
OMP Algorithm

Input: Measurement vector $\mathbf{y} \in \mathbb{C}^K$, sensing matrix $\mathbf{A} \in \mathbb{C}^{K \times N}$, quantization step Δ
Output: Estimated time delays $\{\hat{t}_l\}_{l=1}^L$ and corresponding estimated amplitudes $\{\hat{a}_l\}_{l=1}^L$

```

 $\mathbf{r} \leftarrow \mathbf{y}, \Omega \leftarrow \emptyset$  {Initialization}
 $\text{for } l = 1 \text{ to } L \text{ do}$ 
     $\mathbf{p} = \mathbf{A}^\dagger \mathbf{r}$  {Acquire subspace approximation}
     $\hat{n}_l = \arg \max_{n=1,\dots,N} |p_n|$  {Find maximal component}
     $\Omega \leftarrow \Omega \cup \{\hat{n}_l\}$  {Augment the support set}
     $\hat{t}_l = \hat{n}_l \Delta$ 
     $\mathbf{A}_\Omega \leftarrow [\mathbf{A}_{\hat{n}_1} \cdots \mathbf{A}_{\hat{n}_l}], (\mathbf{A}_n)_m = \mathbf{A}_{m,n}, m = 1, \dots, K$ 
     $\mathbf{P}_\Omega = \mathbf{I} - \mathbf{A}_\Omega \mathbf{A}_\Omega^\dagger$  {Subspace projection operator}
     $\mathbf{r} = \mathbf{P}_\Omega \mathbf{y}$  {Compute the residual}
 $\text{end for}$ 
 $\mathbf{a} = \mathbf{A}_\Omega^\dagger \mathbf{y}$  {Estimate amplitudes via least-squares}

```

C. Frequency Selection

As mentioned previously, CS-based techniques allow flexibility in choosing the Fourier coefficients. Using OMP, high recovery performance is promised, provided that the sensing matrix satisfies desired conditions such as the restricted isometry property (RIP). Selecting the frequency samples uniformly at random, it is known that if

$$K \geq CL(\log N)^4, \quad (6)$$

for some positive constant C , then \mathbf{A} obeys the RIP with high probability [33]. In contrast, for consecutive frequency selection the RIP is not generally satisfied, unless the cardinality of κ is significantly increased. However, applying random frequency sampling is not practical from a hardware perspective, and therefore a rule for selecting a good constellation of frequency samples is desired.

Some practical guidelines for choosing the frequencies are suggested in [34]. The authors consider an equivalent problem to (3), with the roles of frequency and time interchanged. That is, the measurement vector consists of time samples of a signal, described by a spectral line model. Conclusions can be easily adapted to our application with minor changes. Applying these guidelines, we may formalize the following relationship between the support of the recovered signal T , the grid

resolution Δ , and the chosen frequency samples $\{f_i\}_{i=1}^K$:

$$T = \frac{1}{\min_{i,j=1,\dots,K; i \neq j} |f_i - f_j|}, \quad (7)$$

$$\Delta = \frac{1}{c \cdot \max_{i,j=1,\dots,K} |f_i - f_j|}, \quad (8)$$

where c is an empirical constant. In our simulations we set $c = 20$, finding this value to be more robust than that proposed in [34].

Condition (7) constrains us to selecting at least two Fourier coefficients consecutively. In our application, we choose a constellation consisting of four groups of coefficients, where the coefficients in each group are consecutive. We refer to this choice as multiple bandpass sampling. Note that (7) could be equally satisfied by simply using a single group of K consecutive coefficients. As discussed in Section III, such a choice is implemented by simple hardware, consisting of a single low-pass filtering channel. However, our multiple bandpass constellation has the advantage of acquiring the measurements over a wider frequency aperture. At the same time, it still allows practical hardware implementation (as detailed in Section III). Referring to (8), by widening the frequency aperture, we may employ a finer resolution grid during the recovery process. Moreover, empirical results show that highly distributed frequency samples provide better noise robustness [8]. We point out that widening the frequency aperture eventually requires increasing the number of samples K , otherwise recovery performance may degrade. This trade-off, observed in our experiments, is readily seen from (6), where the minimal number of samples K gradually increases with N , corresponding to the grid resolution.

An intuitive explanation for our choice of coefficients may be obtained by adopting insights from the field of array processing. This is because our sampling domain (Fourier coefficients) is related to the parameters' domain (time delays) in the exact same manner in which the geometric sensor deployment pattern in array processing is related to the resulting beampattern. The beampattern determines the angular resolution and ambiguity of the array, which are analogous to temporal resolution and ambiguity in our problem. In particular, narrower array aperture (corresponding to the span of Fourier coefficients) will typically result in a wider mainlobe, providing poorer target resolution, as well as degradation in the accuracy of direction of arrival estimation (DOA) at low SNR. Considering an equally spaced sensor array, one can show that widening the array aperture while maintaining angular ambiguity requires additional sensors; trying to distribute the sensors further apart while keeping their uniform distribution will inevitably affect directional ambiguity. A possible trade-off is to distribute the sensors nonuniformly within the wide aperture, for instance in a pattern chosen randomly, such that the minimal distance between at least two sensors remains fixed [17, 18].

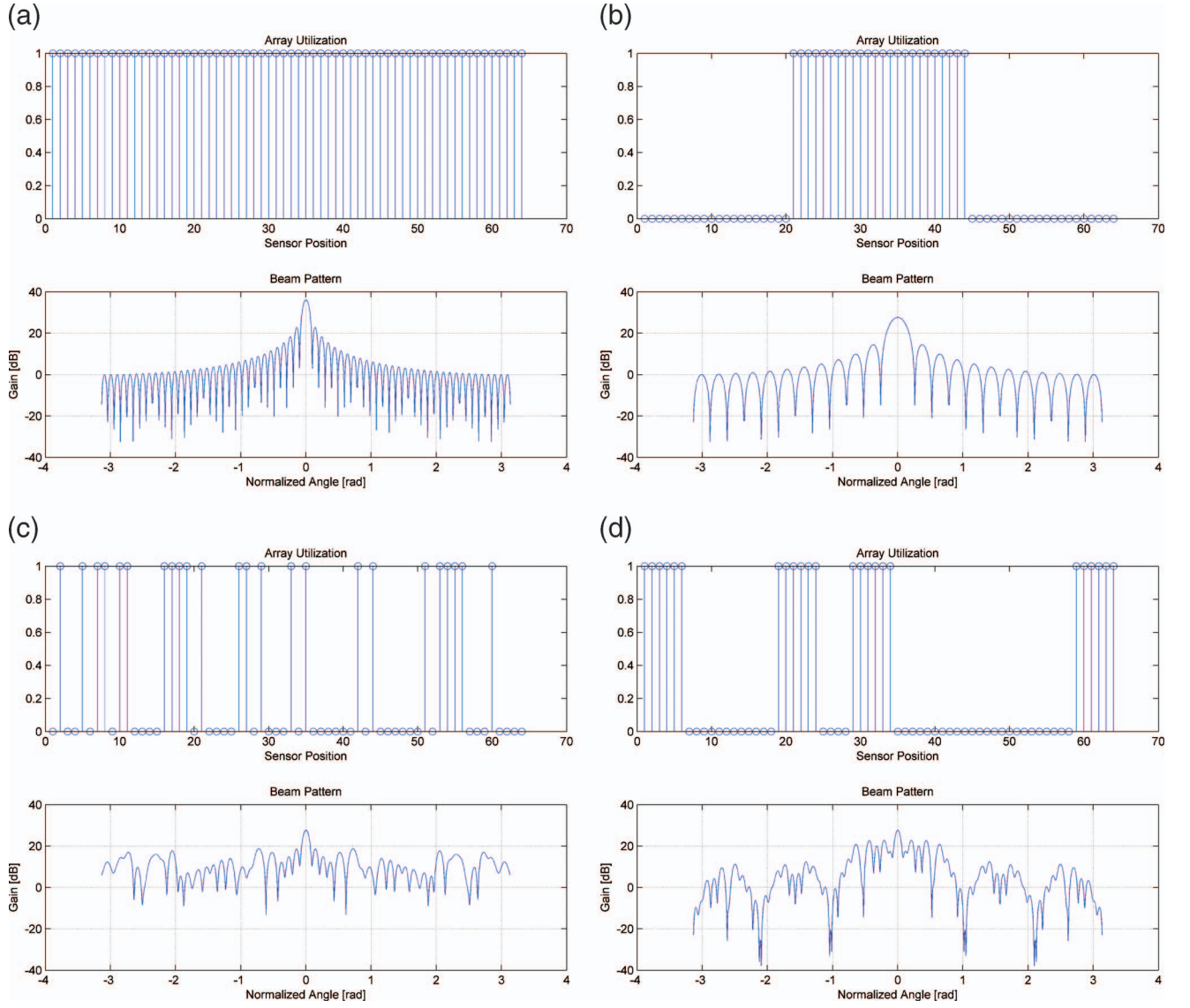


Fig. 1. Beampatterns for different geometries of sensor arrays. Each figure shows array patterns and corresponding beampattern. (a) Full array of 64 sensors. Figs. (b)-(d) correspond to 24 sensors with different distributions. (b) Consecutive. (c) Random. (d) Four randomly distributed groups.

In Fig. 1 we illustrate four choices of sensor patterns, together with the resulting beampatterns. We begin with a uniform array comprising 64 sensors. We then look at three arrays, each employing only 24 sensors: a consecutive array where the sensors are bunched together, a randomly chosen array, and an array comprising 4 groups of size 6 each, where the groups are randomly distributed. The latter constellation resembles the choice of Fourier coefficients in our hardware prototype. The figure illustrates how the nonuniform, randomly chosen distribution of sensors, maintains a narrow mainlobe, at the cost of increased sidelobes. This may result in aliasing of sufficiently strong targets but offers good resolution. Using random groups maintains the narrow mainlobe with a slight increase in sidelobes. From a hardware perspective, this selection is far more practical than a completely random choice. Thus, it offers a reasonable trade-off between performance and hardware design.

III. HARDWARE

We now discuss practical considerations that guided the design of the proposed analog board. We begin by examining previous proposals for sub-Nyquist schemes and point out the difficulty in their direct implementation. We then present our prototype. Throughout this section we consider the following system parameters: A PRI of $T = 1$ ms, which corresponds to 1 KHz spacing of Fourier coefficients. The pulse $h(t)$ is chosen to be approximately flat in spectrum, over the extent of 10 MHz (single-sided band). We assume a maximal number of $L = 6$ targets within the PRI. The desired set of Fourier coefficients is denoted by κ .

A. Previous Work

Extracting a consecutive Fourier subset can be performed using an LPF, followed by sampling at twice its

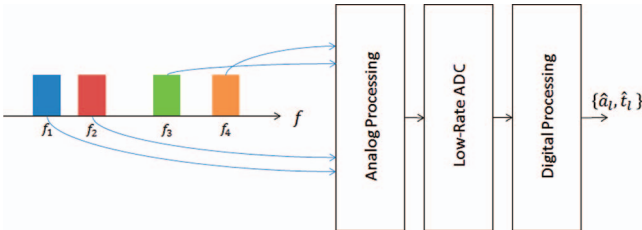


Fig. 2. Xampling of radar signals.

stopband frequency. The DFT of the samples provide the desired Fourier coefficients. However, as discussed in Section II, recovery performance is enhanced when using a set of coefficients distributed over a larger part of the signal's spectrum.

To extract arbitrary sets of Fourier coefficients, [6] introduces a single-channel, presampling filter with frequency response

$$G(f) = \begin{cases} \text{nonzero}, & f = \frac{k}{T}, k \in \kappa \\ 0, & f = \frac{k}{T}, k \in \mathbb{Z} \setminus \kappa \\ \text{arbitrary}, & \text{otherwise.} \end{cases} \quad (9)$$

Implementing a kernel satisfying (9) corresponding to an arbitrary choice of isolated frequency samples requires multiple pass-bands and extremely high frequency selectivity. These characteristics are difficult to satisfy when designing a practical analog filter.

The selectivity property requires high Q-factor filters, with large attenuation within 1 KHz, the coefficients' spacing. Filtering under this regime corresponds to Q-factors on the order of thousands, which is infeasible even when using piezoelectric components. In addition, any off-the shelf filter with high Q-factor will have a long impulse response. This can cause instability when processing multiple pulse-streams. These considerations show that implementing this class of filters with our application's specification is difficult.

An alternative architecture was proposed in [7], which suggests the use of multichannel mixers and integrators to directly compute and sample the Fourier coefficients at a rate of $1/T$ in each channel. In this scheme one channel is needed for each Fourier value, resulting in a large number of channels that must be synchronized and large physical dimensions of the hardware.

B. Multichannel Crystal Receiver

We suggest a multichannel crystal receiver to obtain Fourier coefficients in a manner that is both practical and efficient. This approach makes use of four parallel channels which sample distinct bands of the radar signal spectrum, as illustrated in Fig. 2. Each channel consists of filtering the desired band, demodulating it to baseband and then sampling it at its Nyquist rate. In this scheme, instead of sampling isolated Fourier coefficients, we acquire four sets of consecutive values. This allows to trade off between the theoretical algorithmic requirements, which

benefit from a fully distributed selection, and the constraints of practical analog filters.

In our scenario, the proposed approach achieves a 1 MHz sampling rate (combining all four channels), whereas the Nyquist rate, corresponding to the bandwidth of $h(t)$, is 20 MHz. However, the design of systems for classical methods such as MF, is constrained to the usage of practical filters as well. An antialiasing LPF must be used prior to sampling, and due to the finite width of its transition band, it is not feasible to sample the filter's output at the signal Nyquist's rate without causing aliasing. Modeling an LPF with Chebyshev type-I, and allowing a maximal order of 6, we were able to achieve a stop frequency of 15 MHz, which requires sampling at 30 MHz, a 1.5 oversampling factor with respect to the signal's Nyquist rate. Thus we conclude that our scheme achieves an even greater reduction compared with practical implementation of classical methods.

In order to maintain a low oversampling factor, we employ filters characterized by narrow pass-bands. For instance, with $T = 1$ ms, a 120 KHz pass-band corresponds to 120 Fourier coefficients. This is ten times the minimal number implied by the FRI framework for $L = 6$ pulses in a noiseless scenario. In order to avoid the usage of I/Q channels which, as stated before, adds complexity to the system, we demodulate the band-pass filter's (BPF's) stop frequency in each channel, rather than its central frequency, as done in customary design. This requires that the filters be characterized by narrow transition bands, in order to sufficiently attenuate image frequencies aliasing our chosen coefficients. We observed that active filters satisfying our narrow pass-band requirement yield unsatisfactory attenuation of the image frequencies, degrading the recovery performance. We therefore chose to use crystal filters, whose transition bands are extremely narrow. These filters are characterized by an 80 KHz pass-band. The narrow transition bands allow to achieve low rate sampling, while extracting a sufficient number of Fourier coefficients. Another advantage of the crystal filtering implementation is that it results in identical receiver channels, which have small phase unbalance and are easy to synchronize.

We performed simulations in order to obtain a good combination of the 80 KHz pass-bands in all four channels: multiple constellations of four frequency groups were examined, each obtained by randomly choosing four central frequencies and then taking narrow sets of consecutive coefficients surrounding these frequencies. The following constellation was found to yield good performance, based on the evaluation methods detailed in Section IV: 590 KHz - 670 KHz; 690 KHz - 770 KHz; 1315 KHz - 1395 KHz; 1574 KHz - 1654 KHz.

C. Analog Receiver Design

A full block-diagram of the proposed receiver is depicted in Fig. 3. The system is intended to operate in baseband frequencies, while the receiving and

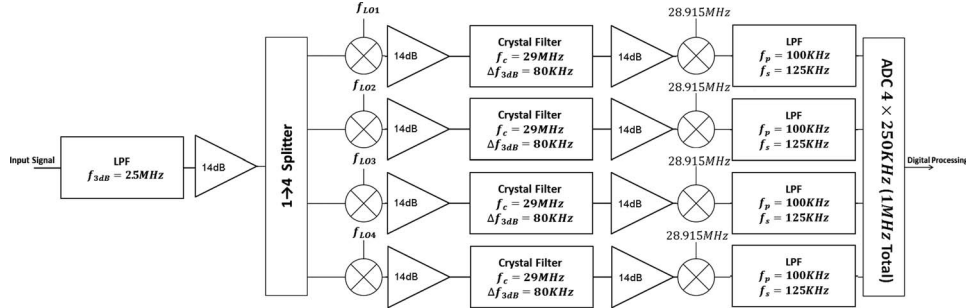


Fig. 3. Block diagram of 4-channel crystal receiver. Four up-modulating LOs have frequency values: $f_{LO1} = 28.375$ MHz, $f_{LO2} = 28.275$ MHz, $f_{LO3} = 27.65$ MHz, $f_{LO4} = 27.391$ MHz.

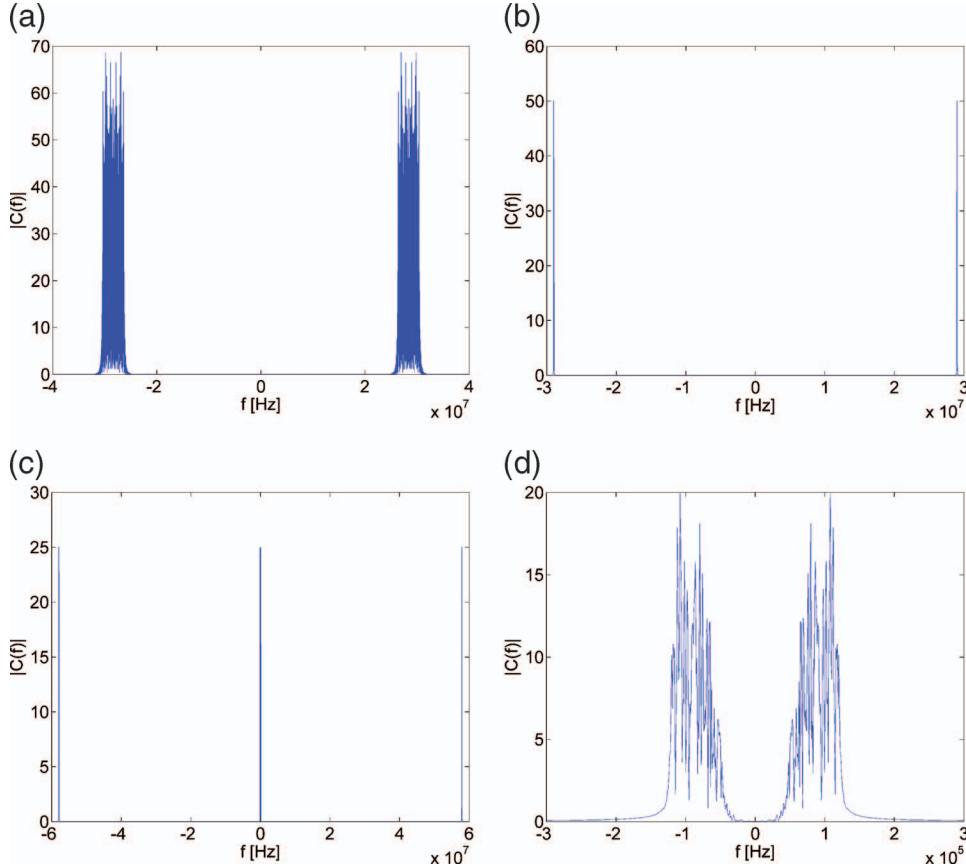


Fig. 4. Dynamics of signal's spectrum through one channel of 4-channel crystal receiver. (a) Signal is modulated to crystal's center frequency. (b) Filtering with narrowband crystal filter. (c) Signal is demodulated to baseband, and high image frequencies appear. (d) Filtering with antialiasing filter to suppress image frequencies.

demodulating of RF signals was simulated in a computer environment (see Section IV). Amplification units were added, in order to compensate for the high losses along each channel. Among the reasons for these losses, are the four-fold signal power reduction at the splitter, the filtering of an 80 KHz slice out of a 10 MHz bandwidth signal, and the total four-fold reduction caused by the up and down conversions. As crystal filters operate only in specific central frequencies, we performed two stages of modulation, in which the desired band is up-converted to the pass-band of the filter and then, after filtering, is demodulated to baseband. It is then filtered with a

125 KHz antialiasing LPF that suppresses the modulation image. The stop frequency was chosen in order to acquire an oversampling margin that allows minimal distortion to the Fourier coefficients lying in the 25 KHz -105 KHz band due to image frequencies or aliasing.

The four-stage process is illustrated in Fig. 4, which shows the dynamics of the signal's spectrum through one of the channels. The final LPF allows sampling each channel at 250 KHz, resulting in a total sampling rate of 1 MHz at all channels combined – a 20-fold reduction relative to the 20 MHz Nyquist rate, and a 30-fold reduction relative to a practical implementation of MF.

TABLE I
Preliminary LPF Specifications

Parameter	Value
Pass Frequency	2.5 MHz
Maximal Pass-band Ripple	1 dB
Stop Frequency	56.35 MHz
Minimal Stopband Attenuation	40 dB

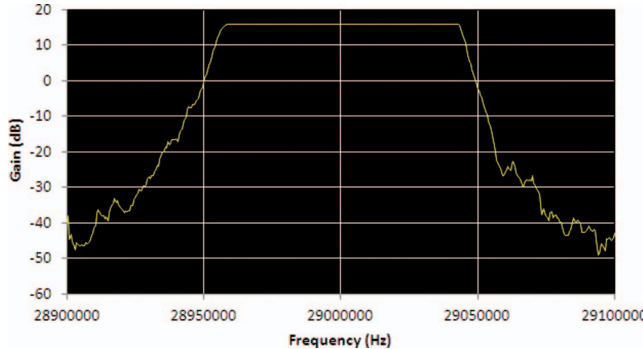


Fig. 5. Magnitude response of crystal BPF as function of frequency.

TABLE II
Crystal Bandpass Filter Characteristics

Parameter	Value
Center Frequency	29 MHz
-3dB Bandwidth	80 KHz
Maximal Pass-band Ripple	1 dB
Stopband Frequencies	28.94 MHz, 29.06 MHz
Minimal Stopband Attenuation	60 dB

Once the channel output is sampled, its spectrum is easily calculated via the fast Fourier transform (FFT) algorithm, and the 320 relevant Fourier coefficients are ready as the recovery algorithm's input.

In our design we make use of three filtering stages. The first stage is located before the mixers in order to suppress image frequencies that may coincide with the desired Fourier coefficients. In the first stage modulation to the crystal pass-band is performed. Since the modulated frequencies and the images vary from channel to channel the specification for the preliminary LPF must be set to the worst case. Thus, the left-most image frequency that modulates our data, which is 56.35 MHz, must be sufficiently suppressed by the LPF. Simulations affirmed that at 40 dB attenuation at this frequency does not affect the performance, and therefore this is the minimal attenuation we require. Table I summarizes the specifications for the preliminary filter.

In the next filtering stage, we make use of crystal filters. As these are standard, off-the-shelf devices, the rest of the stages must be adapted to their properties, while maximizing the channel efficiency (in terms of amount of data acquired and the sampling rate at the ADCs). Fig. 5 shows the magnitude response of a crystal filter, measured in a network-analyzer, and Table II details its properties. With a data bandwidth of 80 KHz on each channel, we are

TABLE III
Antialiasing LPF Specifications

Parameter	Value
Pass Frequency	105 KHz
Maximal Pass-band Ripple	1 dB
Stop Frequency	125 KHz
Minimal Stopband Attenuation	25 dB

able to acquire as many as 320 Fourier coefficients, which allows reconstruction of various scenarios including a different number of targets, varying distances, and a wide RCS range. The narrow transition band of the magnitude response, which achieves 60 dB attenuation at an offset of 60 KHz, allows to demodulate the data band to very low frequencies. In practice, we demodulate the left-most frequency of the pass-band to a frequency of 25 KHz, with the right-most frequency demodulated to 105 KHz. Demodulating the data to the DC frequency is undesirable, since in this case image suppression is not satisfactory.

Finally, sampling the signal requires that we suppress any frequency that might alias our data. Examining Fig. 4(c), it is evident that the main contribution to aliasing occurs from the part of the crystal's pass-band energy that was modulated to very high frequencies. Therefore, it is sufficient to design an antialiasing filter that is efficient enough in suppressing that band. However, each channel incorporates the usage of amplifiers, which have nonlinear regimes. Such nonlinearities may introduce high-order harmonics of the signal, and therefore the antialiasing filter must be designed to suppress any frequency component which we might not have accounted for. Using narrow filters also contributes to noise reduction, which improves the performance of the recovery algorithm. The desired characteristics of the antialiasing LPF are detailed in Table III. With the stop frequency being 125 KHz we are able to sample the output signal at a rate of 250 KHz, which yields a total rate of 1 MHz at all four channels.

Another consideration in the design of the receiver is the noise figure (NF) of the system. The NF measures the degradation of the SNR across the channel. In our design, we make use of operational amplifiers LMH-6629 as power amplifiers, which have a gain of 14 dB and an NF of 9 dB. The mixers have a conversion loss of 5 dB, while the crystal filters have an insertion loss of 4 dB. Splitting the power of the signal to four separate channels yields attenuation of 6.28 dB. The preliminary LPF and the antialiasing LPF have very small insertion loss, and therefore their NFs are negligible. To obtain the total NF of the system, we use the Friis equation [35],

$$NF_{system} = NF_1 + \sum_{n=2}^N \frac{NF_n - 1}{\prod_{m=1}^{n-1} G_m} \quad (10)$$

where G_n and NF_n are the gain and NF of the n th component in the channel, respectively, and N is the number of total components. Incorporating the fact that the NF of an attenuator is equal to its attenuation level, the

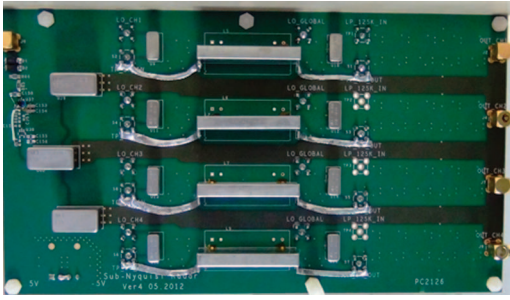


Fig. 6. 4-channel crystal receiver prototype.

total NF of our system is $N F_{\text{system}} = 11$ dB. This causes a degradation that can be compensated by averaging over several periods of the signal, as discussed in Section IV.

A photo of our 4-channel crystal receiver analog board prototype is presented in Fig. 6. In the next section we show real-time experiments of the hardware prototype, and compare its performance with a simple LPF which filters the signal at 500 KHz and samples it at an identical rate of 1 MHz, as well as to the traditional MF which operates at rates higher than Nyquist.

IV. SIMULATIONS AND EXPERIMENTS

In this section we present hardware simulations incorporating practical filtering, as well as real experiments of our hardware prototype that include the transmission of analog signals.

A. Simulations

We first evaluate our hardware and recovery method via MATLAB. We examined the success in recovering multiple realizations of the signal defined in (1), after its corruption by noise. Each realization comprised $L = 6$ pulses. The pulse and its spectrum are depicted in Fig. 7. Time delays and amplitudes were drawn uniformly, at random, within the intervals $[0, 1\text{ms}]$ and $[0.5, 1.5]$, respectively. The signals were generated digitally, at a rate of 0.6 GHz, which is much higher than the Nyquist rate corresponding to $h(t)$'s 10 MHz bandwidth. The signals were corrupted by zero-mean white Gaussian noise, with variance σ^2 determined such that the SNR, defined with respect to the weakest target as

$$\text{SNR} = \frac{1}{\sigma^2} \min_{l=1,\dots,L} |a_l|^2, \quad (11)$$

maintains a predefined value.

To measure the system's recovery performance and to compare it to other solutions, we define the hit-rate and the root-mean-square error (RMSE) metrics in the following manner:

$$\begin{aligned} \text{Hit-Rate} &= \frac{1}{L} |\{\hat{t}_l \mid |\hat{t}_l - t_l| \leq \varepsilon_{th}, l = 1, \dots, L\}| \\ \text{RMSE} &= \left(\frac{1}{L \cdot \text{Hit-Rate}} \sum_{l:|\hat{t}_l-t_l|\leq\varepsilon_{th}} (\hat{t}_l - t_l)^2 \right)^{\frac{1}{2}}, \end{aligned} \quad (12)$$

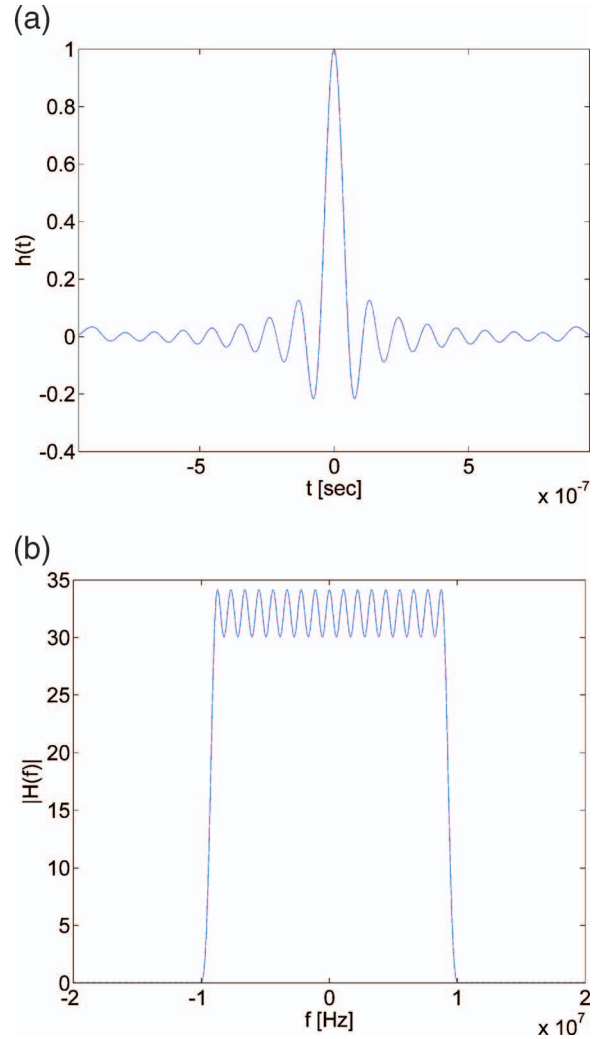


Fig. 7. Temporal shape of pulse (a) and its Fourier spectrum (b).

where $\{\hat{t}_l\}_{l=1}^L$ are the estimated time delays and ε_{th} is the tolerance factor, determined by application (we chose $\varepsilon_{th} = 150$ ns, which is three times the signal's Nyquist period). The RMSE is calculated only with respect to the estimates found within the tolerance interval. In order to obtain statistically stable results, each experiment was repeated 500 times.

We evaluated the performance of four different estimation methods. The first was our 4-channel crystal receiver, where OMP was used for recovering the unknown signal parameters from its subset of Fourier series coefficients. The next two methods were based on a single LPF channel which operates at a total sampling rate of 1 MHz, and obtains a group of consecutive Fourier values. Although the sampling rate at this single channel is 1 MHz, we are only able to extract 400 coefficients due to nonideal transition bands. We considered two different recovery methods: the MP algorithm [31], and OMP. Note that all three of the schemes operate under the same overall sampling rate. Finally, we compared the former approaches with the traditional MF method, which

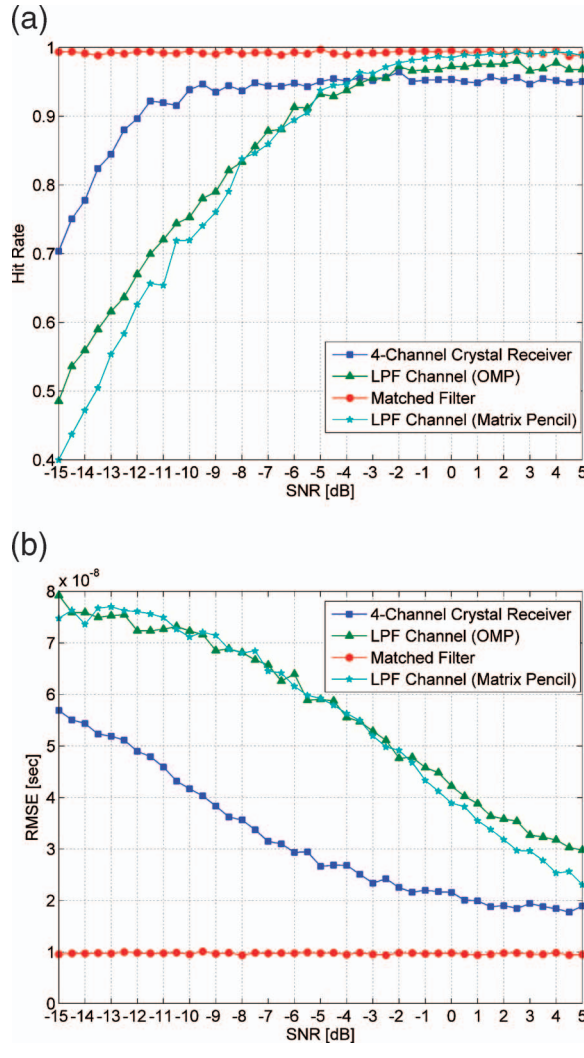


Fig. 8. Comparison of four sampling and estimation methods.
(a) Hit-rate. (b) RMSE. Number of samples per PRI used for processing is: 1000 (crystal receiver, LPF, and MP), 30000 (MF).

requires sampling at a rate 1.5 times higher than the Nyquist rate (30 MHz).

All the filters used in our simulations were modeled via MATLAB's filter design and analysis tool, and were based on the Chebyshev type-I filter. The electronic filters in the different schemes (such as the antialiasing LPFs) were designed so that their order does not increase above 6. In contrast, the crystal filter was modeled with a high order BPF, in order to mimic its narrow transition bands. As part of the digital procedure, we integrated over reflections of 500 consecutive pulses in order to reduce noise power. While this procedure constrains us to slow moving targets, our technique remains applicable to various scenarios, such as naval target, vehicle and human tracking, and more.

Fig. 8 depicts the performance of the four aforementioned methods, as a function of the preintegrated SNR, tested for multiple realizations of our radar signal. Note that two of the methods make use of the same single LPF channel. Examining the results we infer

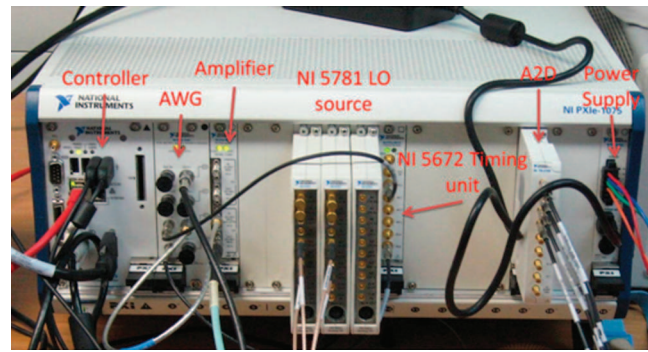


Fig. 9. NI chassis.

TABLE IV
NI PXI Devices

NI Part No.	Description
NI PXIE-1075	18-Slot 3U PXI Express Chassis
NI PXIE-8133	Core i7-820QM 1.73 GHz Controller
NI PXIE-5451	400 MSamp/s Arbitrary Waveform Generator (AWG)
NI PXI-5690	2 Channel RF Preamplifier from 500 KHz to 3.0 GHz
NI PXI-4130	Power SMU
NI PXI-6123	16-Bit, 500 KSamp/s/ch, Simultaneous Sampling Multifunction ADC
NI PXIE-6672	Timing and Multichassis Synchronization Unit for PXI Express
NI 5781	Baseband Transceiver for NI FlexRIO
NI PXI-7965R	NI FlexRIO FPGA Module for PXI

that the 4-channel crystal receiver yields much better performance than LPF-based methods at low SNR values. This corresponds to the fact that in noisy realizations the aperture is critical. As the SNR increases, the aperture plays a less significant role, and the total number of samples determines the reconstruction performance. It is not surprising that the less noisy the samples are, the better the performance obtained by MP. The latter does not quantize the time axis and can reach numerical precision for high enough SNR values [31]. For comparison, the MF curve is also plotted. It is quite clear that it provides better performance than our approach, in particular for low SNR values, but as the SNR improves the performance gap drops. The figure also shows that our 4-channel crystal receiver provides lower RMSE than the LPF-based methods, in the entire SNR range, and approaches the MF performance as the SNR increases.

B. Experimental Environment

To evaluate the board we make use of NI PXI equipment for both system synchronization and signal sources. The entire component ensemble, wrapped in the NI chassis, is depicted in Fig. 9. The components we make use of are listed in Table IV.

In order to achieve system stability, and to obtain fine recovery performance, synchronizing the system is essential. Jitters and drifts between clocks, might skew the time instances in a manner that distorts the calculated Fourier coefficients. We therefore must ensure that our

entire component ensemble, including the arbitrary waveform generator (AWG), local oscillator (LO) signals and ADCs, are triggered by the same clock. This promises that phase unbalance between devices is brought to a minimum.

The advantage of the NI PXI chassis is that it can synchronize several devices to one base clock and distribute a trigger signal with skew less than 1 ns. The ability to synchronize all devices to one clock keeps the jitter between signals low so that we can assume it does not cause a change in phase during operation. Therefore, the whole system is stable and consistent.

C. Experiments

The experimental process consists of the following steps. We begin by using AWR software, which provides the ability to examine a large variety of scenarios, comprising different targets, distances, and RCS values. It is able to simulate the complete radar scenario, including the pulse transmission and accurate power loss due to wave propagation in a realistic medium. It also takes into account the reflections from the unknown targets, which are proportional to their RCS. Finally, AWR software contains a model of a realistic RF receiver, which performs signal processing at high frequencies. The demodulation of the signal to IF frequencies is simulated, and the output is saved to a file. Next, the simulation result is loaded to the AWG module, which produces an analog signal. This signal is amplified using the NI 5690 low noise amplifier (LNA) and then routed to our 4-channel crystal receiver. The receiver is fed by 5 LOs, of which 4 modulate the desired frequency band of each channel individually to the crystal pass-band, and a global one that modulates the latter to a low frequency band, before sampling. The LOs are created using 3 NI 5781 baseband transceivers, acting as trigger-based signal generators with a constant and known phase, controlled by NI Flex Rio field-programmable gate arrays (FPGAs). The AWG also triggers the ADC to sample 250 samples in each sampling cycle, per channel. These samples are fed into the chassis' controller and a MATLAB code is launched that runs the reconstruction algorithm. Our system contains a fully detailed interface implemented in the LabView environment, which allows simple activation of the process. A screenshot of the interface is depicted in Fig. 10.

Performing the previously described processes, we tested various scenarios on the board, that is, a variety of targets, distances, and RCS, and examined the reconstruction quality. Testing the board for its limitations leads to the following results. The minimal voltage for a reconstructible pulse, without PRI integration, is approximately 4 mV, which corresponds to a power of $P_{min} = 320 \text{ nW} = -34.94 \text{ dBm}$. As the board contains amplification units, we must also consider the maximal allowable input power. Above this power, the amplifiers reach their nonlinear regimes and introduce noninvertible

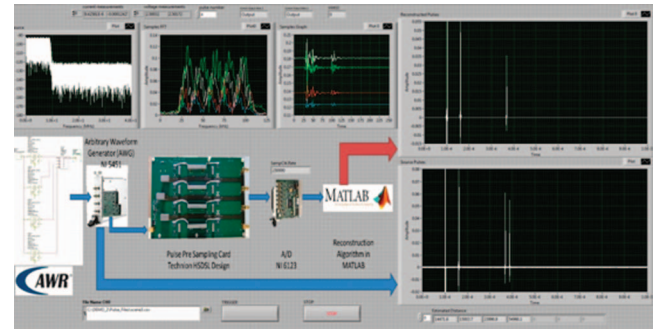


Fig. 10. LabView experimental interface. From left to right: signal's spectrum, frequency response of each channel, 4 signals viewed in each channel, at top - the reconstructed signal, at bottom - the transmitted signal.

distortions to the input signal. Measurements indicate that above a voltage of 92 mV, which corresponds to a power of $P_{max} = 169.28 \mu\text{W} = -7.7139 \text{ dBm}$, such effects begin to take place. We thus deduce that our system has a dynamic range (DR) of

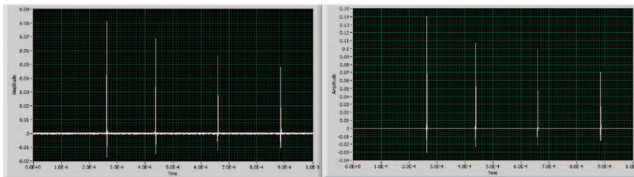
$$DR_{system} = P_{max} - P_{min} = 27.23 \text{ dB}. \quad (13)$$

The DR of the analog system can be digitally enhanced using pulse integration. For example, integrating over 500 pulses, increases the DR by a factor of 10 $\log_{10}(500) = 27 \text{ dB}$.

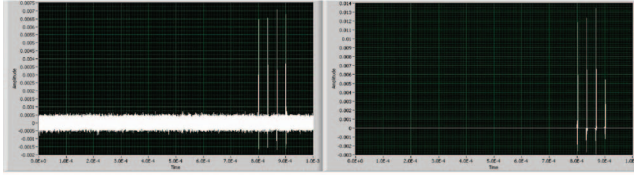
We also tested the limitations for multiple-pulse scenarios. In cases where the OMP algorithm fails to obtain time delays with a small enough error, calculating the residual might yield unsatisfactory attenuation of the part of the measurements corresponding to the located pulse. For pulses energetic enough this means that their residual might still be stronger than the remaining pulses. We measured that a scenario of two pulses with voltage ratio above 12 causes the algorithm to select the stronger pulse twice in consecutive iterations, thus failing to identify the weaker pulse.

Fig. 11 demonstrates our system's reconstruction abilities in 4 target scenarios. In (a), we simulate 4 evenly spaced targets located at distances of 39.28 km, 65.43 km, 98.76 km, 132.54 km. The estimates were calculated as 39.275 km, 65.423 km, 98.752 km, 132.529 km, respectively, providing a maximal error of only 11 m. Fig. 11(b) tests evenly spaced targets at shorter distances. The received pulses correspond to targets at distances 120 km, 125 km, 130 km, 135 km. Note that this experiment shows the system's performance at relatively long distances. Estimated targets were found at 119.99 km, 124.995 km, 129.997 km, 134.981 km, providing a maximal error of 19 m. In (c) we demonstrate the system's DR, as well as its ability to separate close targets. The transmitted pulses correspond to targets located at 72.5 km, 74 km, 76 km, 78 km. To demonstrate the DR, the third target was chosen to have an echo 7 times stronger than the other targets. The system estimated the following distances: 72.499 km, 73.992 km, 75.994 km,

(a)



(b)



(c)

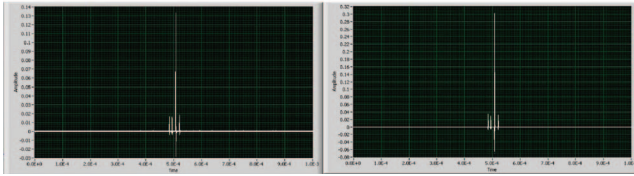


Fig. 11. Signal reconstruction with 4-channel crystal receiver, for different scenarios. Left pane corresponds to received signals, while right pane depicts reconstructed signals.

77.995 km. Furthermore, although the pulses' amplitudes were highly diverse, their estimations were accurate.

V. CONCLUSION

We presented the first sub-Nyquist radar prototype based on the Xampling methodology. We have been able to reduce the total sampling rate by a factor of approximately 30 while maintaining reasonable target location estimation and hit-rate ability. Our experiments with the hardware have further proven that sub-Nyquist sampling of radar signals is possible without losing much of the recovery performance.

In the future, theoretical research might enrich the mathematical model, with the addition of Doppler effects and relaxing the demand that the shape of the pulses is known. Different algorithms and methods might be considered instead of OMP, to increase noise robustness and spatial resolution. We believe that the implementation of a sub-Nyquist radar prototype is an important step towards the incorporation of Xampling and FRI frameworks into real communication and signal-processing systems.

ACKNOWLEDGMENT

The authors would like to thank National Instruments Corporation for their support throughout the development of the prototype, and for their supply of equipment that allowed system operation. Special acknowledgment is due to Mr. Eran Castiel of NI Israel, Dr. Ahsan Aziz of NI Texas, and the entire support group of NI Israel, for their

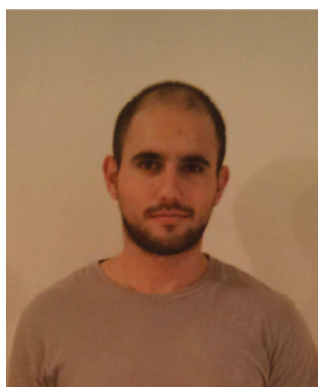
efforts and cooperation with the sub-Nyquist group at the Technion.

The authors would also like to thank Dr. Eyal Doron of Pearls of Wisdom, Advanced Technologies, Kefar Netter, Israel, for sharing valuable insights from the field of array processing and for many helpful discussions.

REFERENCES

- [1] Cook, C. E. Pulse compression - Key to more efficient radar transmission. *Proceedings of the IRE*, **48**, 3 (1960), 310–316.
- [2] Richards, M. A. *Fundamentals of Radar Signal Processing*. New York: McGraw-Hill, 2005.
- [3] Shannon, C. E. Communication in the presence of noise. *Proceedings of the IRE*, **37**, 1 (1949), 10–21.
- [4] Bajwa, W. U., Gedalyahu, K., and Eldar, Y. C. Identification of parametric underspread linear systems and super-resolution radar. *IEEE Transactions on Signal Processing*, **59**, 6 (2011), 2548–2561.
- [5] Stoica, P., and Moses, R. L. *Introduction to Spectral Analysis*. Upper Saddle River, NJ: Prentice-Hall, 1997.
- [6] Tur, R., Eldar, Y. C., and Friedman, Z. Innovation rate sampling of pulse streams with application to ultrasound imaging. *IEEE Transactions on Signal Processing*, **59**, 4 (2011), 1827–1842.
- [7] Gedalyahu, K., Tur, R., and Eldar, Y. C. Multichannel sampling of pulse streams at the rate of innovation. *IEEE Transactions on Signal Processing*, **59**, 4 (2011), 1491–1504.
- [8] Wagner, N., Eldar, Y. C., and Friedman, Z. Compressed beamforming in ultrasound imaging. *IEEE Transactions on Signal Processing*, **60**, 9 (2012), 4643–4657.
- [9] Vetterli, M., Marziliano, P., and Blu, T. Sampling signals with finite rate of innovation. *IEEE Transactions on Signal Processing*, **50**, 6 (2002), 1417–1428.
- [10] Mishali, M., Eldar, Y. C., Dounaevsky, O., and Shoshan, E. Xampling: Analog to digital at sub-Nyquist rates. *IET Journal of Circuits, Devices and Systems*, **5**, 1 (2011), 8–20.
- [11] Mishali, M., Eldar, Y. C., and Elron, E. Xampling: Signal acquisition and processing in union of subspaces. *IEEE Transactions on Signal Processing*, **59**, 10 (2011), 4719–4734.
- [12] Candes, E. J., and Wakin, M. B. An introduction to compressive sampling. *IEEE Signal Processing Magazine*, **25**, 2 (Mar. 2008), 21–30.
- [13] Eldar, Y. C., and Kutyniok, G. *Compressed Sensing: Theory and Applications*. New York: Cambridge University Press, 2012.
- [14] Duarte, M. F., and Eldar, Y. C. Structured compressed sensing: From theory to applications. *IEEE Transactions on Signal Processing*, **59**, 9 (2011), 4053–4085.
- [15] Eftekhar, A., Romberg, J., and Wakin, M. B. Matched filtering from limited frequency samples. *IEEE Transactions on Information Theory*, **59**, 6 (June 2013), 3475–3496.

- [16] Rudelson, M., and Vershynin, R.
On sparse reconstruction from Fourier and Gaussian measurements.
Communications on Pure and Applied Mathematics, **61**, 8 (2008), 1025–1045.
- [17] Lo, Y.
A mathematical theory of antenna arrays with randomly spaced elements.
IEEE Transactions on Antennas and Propagation, **AP-12**, 3 (1964), 257–268.
- [18] Rossi, M., Haimovich, A., and Eldar, Y. C.
Spatial compressive sensing for MIMO radar.
IEEE Transactions on Signal Processing, **62**, 2 (Jan. 2014), 419–430.
- [19] Mallat, S. G., and Zhang, Z.
Matching pursuits with time-frequency dictionaries.
IEEE Transactions on Signal Processing, **41**, 12 (Dec. 1993), 3397–3415.
- [20] Tropp, J. A., and Gilbert, A. C.
Signal recovery from random measurements via orthogonal matching pursuit.
IEEE Transactions on Information Theory, **53**, 12 (2007), 4655–4666.
- [21] Herman, M. A., and Strohmer, T.
High-resolution radar via compressed sensing.
IEEE Transactions on Signal Processing, **57**, 6 (2009), 2275–2284.
- [22] Demissie, B.
High-resolution range-Doppler imaging by coherent block-sparse estimation.
International Workshop on Compressed Sensing Applied to Radar, May 2012.
- [23] Baraniuk, R. G., and Steeghs, P.
Compressive radar imaging.
IEEE Radar Conference, Waltham, MA, Apr. 2007.
- [24] Zhang, J., Zhu, D., and Zhang, G.
Adaptive compressed sensing radar oriented toward cognitive detection in dynamic sparse target scene.
IEEE Transactions on Signal Processing, **60**, 4 (Apr. 2012), 1718–1729.
- [25] Berger, C. R., Zhou, S., and Willett, P.
Signal extraction using compressed sensing for passive radar with OFDM signals.
2008 11th International Conference on Information Fusion, 2008, pp. 1–6.
- [26] Ender, J. H. G.
On compressive sensing applied to radar.
Signal Processing, **90**, 5 (2010), 1402–1414.
- [27] Laska, J. N., Kirolos, S., Duarte, M. F., Ragheb, T. S., Baraniuk, R. G., and Massoud, Y.
Theory and implementation of an analog-to-information converter using random demodulation.
Proceedings of IEEE International Symposium on Circuits and Systems (ISCAS 2007), May 2007, pp. 1959–1962.
- [28] Yoo, J., Turnes, C., Nakamura, E. B., Le, C. K., Becker, S., Sovero, E. A., Wakin, M. B., Grant, M. C., Romberg, J., Emami-Neyestanak, A., and Candes, E.
A compressed sensing parameter extraction platform for radar pulse signal acquisition.
IEEE Journal on Emerging and Selected Topics in Circuits and Systems, **2**, 3 (Sept. 2012), 626–638.
- [29] Chen, X., Yu, Z., Hoyos, S., Sadler, B. M., and Silva-Martinez, J.
A sub-Nyquist rate sampling receiver exploiting compressive sensing.
IEEE Transactions on Circuits and Systems I: Regular Papers, **58**, 3 (2011), 507–520.
- [30] Bar-Ilan, O., and Eldar, Y. C.
Sub-Nyquist radar via Doppler focusing.
IEEE Transactions on Signal Processing, 2013, submitted for publication.
- [31] Sarkar, T. K., and Pereira, O.
Using the matrix pencil method to estimate the parameters of a sum of complex exponentials.
IEEE Antennas and Propagation Magazine, **37**, 1 (1995), 48–55.
- [32] Schmidt, R.
Multiple emitter location and signal parameter estimation.
IEEE Transactions on Antennas and Propagation, **34**, 3 (Mar. 1986), 276–280.
- [33] Vershynin, R.
Introduction to the non-asymptotic analysis of random matrices. In Y. Eldar and G. Kutyniok (Eds.),
Compressed Sensing: Theory and Applications. New York: Cambridge University Press, 2012, ch. 5.
- [34] Stoica, P., and Babu, P.
Sparse estimation of spectral lines: Grid selection problems and their solutions.
IEEE Transactions on Signal Processing, **60**, 2 (2012), 962–967.
- [35] Friis, H. T.
Noise figures of radio receivers.
Proceedings of the IRE, **32** (1944), 419–422.



Eliahu Baransky received his B.Sc. degree in electrical engineering and the B.Sc. degree in physics both from the Technion-Israel Institute of Technology, Haifa, Israel in 2012. He is currently studying for his M.Sc. degree in electrical engineering in the Technion Department of Electrical Engineering.



Gal Itzhak received his B.Sc. degree in electrical engineering and the B.Sc. degree in physics both from the Technion-Israel Institute of Technology, Haifa, Israel in 2012. He is currently studying for his M.Sc. degree in electrical engineering in the Technion Department of Electrical Engineering.

Yonina C. Eldar (S'98—M'02—SM'07—F'12) received the B.Sc. degree in physics and the B.Sc. degree in electrical engineering both from Tel-Aviv University (TAU), Tel-Aviv, Israel, in 1995 and 1996, respectively, and the Ph.D. degree in electrical engineering and computer science from the Massachusetts Institute of Technology (MIT), Cambridge, in 2002.

From Jan. 2002 to July 2002, she was a Postdoctoral Fellow at the Digital Signal Processing Group at MIT. She is currently a Professor in the Department of Electrical Engineering at the Technion-Israel Institute of Technology, Haifa and holds The Edwards Chair in Engineering. She is also a Research Affiliate with the Research Laboratory of Electronics at MIT and a Visiting Professor at Stanford University, Stanford, CA. Her research interests are in the broad areas of statistical signal processing, sampling theory and compressed sensing, optimization methods, and their applications to biology and optics.

Dr. Eldar was in the program for outstanding students at TAU from 1992 to 1996. In 1998, she held the Rosenblith Fellowship for study in electrical engineering at MIT, and in 2000, she held an IBM Research Fellowship. From 2002 to 2005, she was a Horev Fellow of the Leaders in Science and Technology program at the Technion and an Alon Fellow. In 2004, she was awarded the Wolf Foundation Krill Prize for Excellence in Scientific Research, in 2005 the Andre and Bella Meyer Lectureship, in 2007 the Henry Taub Prize for Excellence in Research, in 2008 the Hershel Rich Innovation Award, the Award for Women with Distinguished Contributions, the Muriel & David Jacknow Award for Excellence in Teaching, and the Technion Outstanding Lecture Award, in 2009 the Technions Award for Excellence in Teaching, in 2010 the Michael Bruno Memorial Award from the Rothschild Foundation, and in 2011 the Weizmann Prize for Exact Sciences. In 2012 she was elected to the Young Israel Academy of Science and to the Israel Committee for Higher Education, and elected an IEEE Fellow. In 2013 she received the Technion's Award for Excellence in Teaching, the Hershel Rich Innovation Award, and the IEEE Signal Processing Technical Achievement Award. She received several best paper awards together with her research students and colleagues. She is a Signal Processing Society Distinguished Lecturer, and Editor-in-Chief of *Foundations and Trends in Signal Processing*. In the past, she was a member of the IEEE Signal Processing Theory and Methods and Bio Imaging Signal Processing technical committees, and served as an associate editor for the *IEEE Transactions on Signal Processing*, the *EURASIP Journal of Signal Processing*, the *SIAM Journal on Matrix Analysis and Applications*, and the *SIAM Journal on Imaging Sciences*.

